

Warm dark matter model with a few keV mass is bad for the too-big-to-fail problem

Xi Kang^{1,2} *

¹*Purple Mountain Observatory, No 8 Yuanhua Road, Nanjing 210034, China*

²*Zhejiang University-Purple Mountain Observatory Joint Research Center for Astronomy, Zhejiang University, Hangzhou 310027, China*

Accepted xxxx. Received xxxx; in original form xxxx

ABSTRACT

Theoretical studying of the very inner structure of faint satellite galaxy requires very high-resolution hydro-dynamical simulations with realistic model for star formation, which are beginning to emerge recently. In this work we present an analytical description to model the inner kinematic of satellites in the Milky Way (MW). We use a Monte-Carlo method to produce merger trees for MW mass halo and analytical models to produce stellar mass in the satellite galaxies. We consider two important processes which can significantly modify the inner mass distribution in satellite galaxy. The first is baryonic feedback which can induce a flat inner profile depending on the star formation efficiency in the galaxy. The second is the tidal stripping to reduce and re-distribute the mass inside satellite. We apply this model to MW satellite galaxies in both CDM and thermal relic WDM models. It is found that tidal heating must be effective to produce a relatively flat distribution of the satellite circular velocities, to agree with the data. The constraint on WDM mass depends on the host halo mass. For a MW halo with dark matter mass lower than $2 \times 10^{12} M_{\odot}$, a 2 keV WDM model can be safely excluded as the predicted satellite circular velocities are systematically lower than the data. For WDM with mass of 3.5 keV, it requires the MW halo mass to be larger than $1.5 \times 10^{12} M_{\odot}$, otherwise the 3.5 Kev model can also be excluded. Our current model can not constrain the WDM model with mass larger than 10 Kev.

Key words: methods: numerical — methods: statistical — galaxies: haloes — Galaxy: halo — cosmology: dark matter

1 INTRODUCTION

The Milky Way (MW) is an ideal local laboratory to test the nature of dark matter and galaxy formation physics, as its proximity allows for accurate measurements of the mass and velocity distributions of the satellite galaxies. The two well-known challenges on the cold dark matter (CDM) model are the missing satellite problem which states that the CDM model predicts hundred of subhaloes but only a dozen classical satellite galaxies are observed (Klypin et al. 1999), and the too-big-to-fail problem (TBTf) stating that the most massive subhaloes are too centrally dense to host the brightest satellite galaxies (Boylan-Kolchin et al. 2011). These problems have produced a larger number of studies in the past years. For a recent review on this topic, we refer the readers to the paper by Bullock & Boylan-Kolchin (2017).

To rescue the classical CDM model, the most com-

mon solution is invoking baryonic effects. It was early proposed that the cosmic re-ionization can effectively suppress the gas accumulation in low-mass halo (e.g., Gnedin 2000) and galaxy formation models which include this effect can well match the luminosity and spatial distribution of the satellite galaxies in the MW (e.g., Macciò et al. 2010). On the other hand, the baryonic feedback from star formation can also produce a core-like profile in satellite galaxies to alleviate the TBTf problem (e.g., Governato et al. 2012; Brooks & Zolotov 2014). Other dynamical effects, such as MW disc heating and tidal stripping, are also helpful to lower the central density profile of satellite galaxies and some studies claim such an effect is more efficient in satellites with an initial shallower profile (e.g., Zolotov et al. 2012; Ogiya & Burkert 2015; Dutton et al. 2016; Sawala et al. 2016; Tomozeiu et al. 2016).

Along with the efforts of invoking baryonic feedback in CDM, an alternative solution is to change the properties of dark matter, such as the self-interacting cold dark

* E-mail:kangxi@pmo.ac.cn

matter (e.g., [Vogelsberger et al. 2012](#)), the warm dark matter (e.g., [Polisensky & Ricotti 2011](#)) or the combination of both ([Cyr-Racine et al. 2016](#); [Vogelsberger et al. 2016](#)). These alternative dark matter models seem to be more promising as they can reduce both the number of subhaloes and their central density ([Bode et al. 2001](#); [Colin et al. 2000](#); [Vogelsberger et al. 2019](#)). For the WDM model, constraints based on satellite counts and kinematics are getting stronger. For example, using the satellites count of the MW as a constraint, a few studies ([Macciò & Fontanot 2010](#); [Polisensky & Ricotti 2011](#); [Lovell et al. 2014](#)) have found that a thermal relic warm dark matter candidate with mass $m_\nu > 1 - 2.3$ keV is needed, as a lower mass candidate will produce too few satellite galaxies than observed. Similar constraint is also obtained by [Kang et al. \(2013\)](#) using a joint constraints from local galaxy stellar mass function and the Tully-Fisher relation. On the other hand, [Shao et al. \(2013\)](#) found that a WDM mass around ~ 0.5 keV is needed to produce a density core consistent with the satellite kinematics. [Lovell et al. \(2012\)](#) used N-body simulation to show that a WDM mass with $m_\nu \sim 2$ keV is needed to alleviate the TBTF problem. Thus, the most possible WDM mass around ~ 2 keV is required to simultaneously match the number counts and kinematics of the Milky Way satellites. However, this is in disagreement with the constraint on the WDM mass with $m_\nu > 3.3$ keV using Ly- α forest observations (e.g., [Viel et al. 2013](#)) though this constraint is affected by the thermal history of the intergalactic medium ([Garzilli et al. 2017](#)).

Regardless of the nature of dark matter, most studies have reached consensus that reproducing the satellite luminosity distribution is key to the TBTF problem. In particular, the degree to which haloes have shallower density profiles than expected in CDM or even a central core, if cores indeed exist in nature, is found to be strongly correlated with the star formation efficiency in the satellite using hydrodynamical simulations (e.g., [Di Cintio et al. 2014](#); [Tollet et al. 2016](#); [Fitts et al. 2017](#)) while other simulations suggest that core creation is not an inevitable outcome but depending on star formation history and subgrid physics ([Grand et al. 2017](#); [Bose et al. 2019](#)). In addition, to resolve the very inner kinematic structure of satellites, one need to simulate their evolution with very high spatial- and mass resolution. Putting together, it requires simulation to simultaneously reproduce the stellar mass and kinematics of the MW satellites. Such an effort is only recently achieved from the state-of-the-art hydrodynamical simulations, such as NIHAO ([Wang et al. 2015](#); [Buck et al. 2019](#)), APOSTLE ([Sawala et al. 2016](#)) and FIRE-2 project ([Wetzel et al. 2016](#); [Garrison-Kimmel et al. 2019](#)). These simulations claimed that the two problems can be simultaneously solved and they suggested that tidal stripping and heating, not baryonic feedback, is the main process leading to lower velocity dispersion of satellites. As the tidal effects depend on the inner mass distribution in satellite galaxy (e.g., [Peñarrubia et al. 2010](#)) which is therefore affected by baryonic feedback, one needs controlled simulations to separate the baryonic feedback and tidal process so as to claim which one is the dominant.

Undoubtedly, hydrodynamical simulation is the best tool to address the satellite problems. However, the high computational cost has hindered the accomplishment of a large sample of MW analogous to capture the formation

history of the MW. Given the limited realistic samples and the uncertainty in subgrid physics in the present hydrodynamical simulations, it is still not clear what is the main physical process, either feedback induced core or tidal stripping, to account for the lower mass density in observed satellite galaxies. To this end, analytical model, which can easily follow the formation history of large sample of MW analogous and include relevant baryonic process, is particularly desired. In this work, we aim to construct such a model based on current results. We then apply the model to both CDM and WDM models to investigate the separate effect of feedback induced core and tidal stripping on the satellite kinematics, and in particularly, to set constraints on the mass of the thermal relic WDM model.

Our analytical model contains the following basic ingredients. To model the formation history of the MW type halo, we use the Monte-Carlo code by [Parkinson et al. \(2008\)](#) to produce a large sample of merger trees for MW analogs. To set the stellar mass of satellite galaxies, we use either the semi-analytical model ([Kang et al. 2012](#)) or a simple abundance matching method. To model the kinematics of the satellite galaxies, we follow three steps. Firstly, we assume that before satellite is accreted, its DM distribution initially follows a NFW profile. Secondly, we modify the inner slope of the satellite using the fitted relation between the density slope and the star formation efficiency in satellite galaxy (e.g., [Di Cintio et al. 2014](#)). Thirdly, after satellite is accreted by the host galaxy, tidal stripping from host galaxy will strip the DM mass of the satellite and the associated tidal heating will also alter its inner mass distribution. To model this process, we use the model for the average mass loss of subhalo by [Giocoli et al. \(2008\)](#) and use the fitting formula by [Peñarrubia et al. \(2010\)](#) to model the effect of tidal stripping on the inner density structure of the satellite. With the above procedure, we are then able to predict the circular velocity of satellite at any given radius and compare the model predictions to the data.

Our model is in spirit similar to the recent work by [Lovell et al. \(2017\)](#) in which they also use analytical model to address the satellite kinematics, particularly in the WDM model. Our model is different from theirs in many details. For example, they use the simulation results of [Sawala et al. \(2016\)](#) to include the baryonic effect on the maximum circular velocity V_{max} of the satellite galaxy, and compare the distribution of V_{max} with that obtained for the MW satellites. In our model, the baryonic effect is reflected in the change of the inner density profile which depends on satellite star formation efficiency (e.g., [Di Cintio et al. 2014](#); [Fitts et al. 2017](#)). In fact, the baryonic effect in these based simulations are very different and there is no core creation in the [Sawala et al. \(2016\)](#) simulation. Furthermore, V_{max} is not directly observed for the satellites and there is significant scatter on the derived V_{max} from the observed circular velocities ([Sawala et al. 2016](#)). While in our model we directly compare the circular velocity to the data and it requires us to model the inner slope of the satellites. In addition, the modelling of tidal effect on satellite mass distribution is also different between the two models.

The paper is organized as follows. In Sec. 2 we introduce our analytical method including the production of halo merger trees, method to assign density profile of subhalo before infall, analytical model of star formation for the satellite

galaxies and the modification of their inner slopes by supernova feedback and tidal effect. We present the comparison with the data in Sec. 3 and conclude with short discussion in Sec. 4.

2 ANALYTICAL METHODS

Modelling the properties of observed satellite galaxies in the MW requires accurate information of the formation history of the MW, such as the mass growth of the host halo, the infall time and orbits of the satellite galaxies. Current studies have been trying to derive these information (e.g., Rocha et al. 2012; Simon 2018), but accurate recovery of the infall history of the satellites is still challenging. So we produce a large sample of MW-mass halo around $10^{12} M_{\odot}$ using Monte-Carlo based method. We then model the formation and evolution of luminous satellite galaxy using an analytical model or using a simple abundance matching method to assign stellar mass to the subhalo. For each observed satellite galaxy, we select its counterparts from our model with similar luminosity or stellar mass, and compare the observed properties of the satellite galaxy to the statistical distribution of these model satellites.

2.1 merger tree of MW type halo

We use the Monte-Carlo merger tree code from Parkinson et al. (2008) to produce the formation history of MW-type halo with mass of $10^{12} M_{\odot}$ in both the CDM and WDM models. This algorithm is based on the extended Press-Schechter formalism and revised to match the halo merger tree from Millennium Simulation (Springel et al. 2005). Cole et al. (2008) have shown the improvement from this Monte-Carlo algorithm. The basic input of this method is the analytical power spectrum (e.g., Bardeen et al. 1986) and the cosmological parameter for which we use the WMAP9 cosmology (Hinshaw et al. 2013). We produce 5000 realizations of the merger tree for the MW-type halo.

In the WDM case, the velocity dispersion of DM particles produces a characteristic free-streaming scale below which the structure is suppressed. The lighter the particle mass is, the larger the free-streaming scale. The impact of free streaming on the power spectrum is to modify the transfer function in WDM as suggested in Bode et al. (2001),

$$T(k) = \left(\frac{P_{Lin}^{WDM}}{P_{Lin}^{CDM}} \right)^{1/2} = (1 + (\alpha k)^{2\mu})^{-5/\mu} \quad (1)$$

where P_{Lin}^{WDM} and P_{Lin}^{CDM} are the linear power spectrums in WDM and CDM model. Viel et al. (2005) obtained $\mu = 1.2$ and found that α is related to the WDM mass, m_{ν} , as the following,

$$\alpha = 0.049 \left(\frac{m_{\nu}}{1 \text{ keV}} \right)^{-1.11} \left(\frac{\Omega_{\nu}}{0.25} \right)^{0.11} \left(\frac{h}{0.7} \right)^{1.22} h^{-1} \text{ Mpc}, \quad (2)$$

We use the above equations to derive the initial power spectrum for the WDM model. As noted by Kennedy et al. (2014), also see Benson et al. (2013), the usually adopted top-hat filter is not applicable in the presence of a cutoff in the power spectrum, as was in the WDM case, and a sharp filter in k -space is used instead. We refer the readers

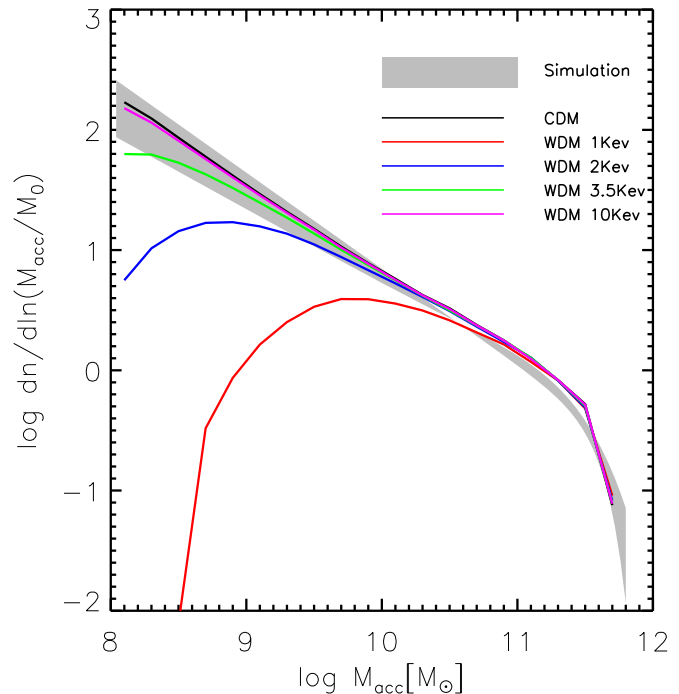


Figure 1. The mass function of accreted subhaloes by a Milky Type host halo with mass around $10^{12} M_{\odot}$. The black line is for CDM and color lines are for the WDM models using the transfer function (Eq. 1 and Eq. 2) with different mass. The hatched gray regions show the results from CDM simulations.

to the Kennedy et al. (2014) paper for detail. In this work, we consider a few WDM mass, with $m_{\nu} = 1, 2, 3.5, 10$ keV. For each WDM mass, we also generate 5000 merger trees for the MW-type host halo with $M_{vir} = 10^{12} M_{\odot}$.

To see the effect of suppressed power spectrum at small scales on the satellite galaxy population in the WDM model, it is firstly useful to see on which scale the formation of low-mass haloes is reduced. In Fig. 1, we show the mass functions of accreted subhaloes by the host halo during its formation history in the CDM and WDM models using the power spectrum from Eq. 1 and Eq. 2. The hatched gray region shows the simulation results from Gao et al. (2004) and Stewart et al. (2008) for CDM model. It is seen that in the WDM model, the formation of low-mass haloes is suppressed and the extent of suppression is dependent on the particle mass. One direct consequence of this result is that, for a fixed star formation efficiency (stellar mass to halo mass relation), the number of luminous satellites would be less in the WDM model. However, given the current uncertainty in star formation model, we will try to match the observed satellite luminosity function by tuning the free parameters in the galaxy formation model as introduced below. Even so, we will find that the WDM model with lower particle mass ($m_{\nu} < 3.5$ keV) is difficult to produce enough faint satellite galaxies.

2.2 Model for galaxy formation

One key ingredient of our model is to set the inner structure of the satellites. As previous introduced, the inner density profile of satellite galaxy will be affected by the baryonic

feedback. To this end, we firstly need to determine both dark matter halo mass and the stellar mass of the satellite galaxies. We use two methods to assign stellar mass to dark matter subhalo. The first one is the semi-analytical model (SAM) of [Kang et al. \(2012\)](#) which is an updated version of our previous model ([Kang et al. 2005](#); [Kang 2009](#)). The SAM includes key processes governing galaxy formation, such as gas cooling, star formation, supernova feedback. We refer the readers to the paper by [Kang et al. \(2005\)](#) for details. In [Kang \(2009\)](#) we included a model for the effect of cosmic reionization on the hot gas content of low-mass haloes (e.g., [Gnedin 2000](#)), by using a filtering mass which corresponds to a mass scale at which haloes will only be able to accrete half of the universal baryonic fraction. The fraction of baryons that can be accreted as hot gas is parameterized as,

$$f_{b,acc}(z, M_{vir}) = \frac{f_b}{[1 + 0.26M_F(z)/M_{vir}]^3} \quad (3)$$

where f_b is the universal baryon fraction and M_{vir} is the virial mass of the halo, and the filter mass $M_F(z)$ is given by [Kravtsov et al. \(2004\)](#). For both the CDM and WDM models, we tune the model parameters, such as star formation and supernova feedback efficiency, to best match the stellar luminosity function of satellites in the MW ([Koposov et al. 2008](#)). The results will be shown in Sec. 3. By doing so, we can get the stellar mass, M_* , for each satellite as well as its virial mass M_{vir} at accretion time.

Another method to select satellite galaxy is similar to the halo abundance matching method (e.g., [Vale & Ostriker 2004](#)). However, many studies (e.g., [Guo et al. 2015](#); [Brook & Di Cintio 2015](#); [Errani et al. 2018](#)) have shown that for satellites of the MW, there is a large scatter between subhalo mass and stellar mass, mainly due to the effect of cosmic reionization on the gas content of low-mass haloes, thus the most luminous satellites do not often live in the most massive subhaloes. However, the TBTF problem concerns more about the kinematic match between the simulated massive subhaloes with the observed luminous satellites. Thus following the spirit of abundance matching (AM) method, we take the nine subhaloes with most massive mass at accretion, but assign the observed stellar mass of the MW satellites (e.g., [Misgeld & Hilker 2011](#)) to these subhaloes, by putting the most luminous satellites to the most massive subhaloes at accretion. We have also tested that our results are not significantly affected if we instead use the highest maximum velocity of subhalo at infall. Given the stellar mass, halo mass and infall times of these satellites, we can use the following descriptions to determine their inner structures and circular velocities.

2.3 Halo density profile and baryonic effect

To predict the circular velocity of satellite galaxy at given radius, we need to specify its density profile. We consider two main process which will modify the mass and dynamical structure of the satellite galaxy: baryonic feedback and tidal stripping. We assume that before satellite is accreted, the main process in play is baryonic feedback which acts to change the inner profile of the galaxy. After accretion, the tidal force from the host halo will strip the DM mass of

the satellite and the associated tidal heating will also continuously re-distribute the mass inside the satellite. In this section we introduce how to include the first effect. We assume that before accretion, the dark matter halo of satellite initially follows a general NFW profile or the so-called α -model ([Ogiya & Burkert 2015](#)),

$$\rho(r) = \frac{\rho_0 r_0^3}{r^\alpha (r + r_0)^{3-\alpha}} \quad (4)$$

where α , ρ_0 and r_0 are the logarithmic slope of the central density, the scale density and scale length. In this description, $\alpha = 1$ corresponds to the classical NFW profile ([Navarro et al. 1997](#)), and $\alpha = 0$ corresponds to a central core. Numerous studies have been devoted to fit α in dark matter only simulations, which is found to be between 1 and 1.5 (e.g., [Moore et al. 1999](#); [Jing & Suto 2000](#); [Diemand et al. 2008](#)). Using more high-resolution simulations (e.g., [Springel et al. 2008](#)), it is shown that the halo mass density is better described by the [Einasto \(1965\)](#) profile with the power index being a function of radius, but NFW still gives a reasonable description to the simulation result. In our calculation we assume that, before invoking baryonic feedback, all haloes have an initial slope with $\alpha = 1$.

To predict the circular velocity using Eq. 4, one needs to specify the halo concentration, $c = R_{vir}/r_0$. In the CDM model, halo concentration, c_{CDM} , is dependent on halo mass and formation time (e.g., [Bullock et al. 2001](#); [Zhao et al. 2003](#)) and a few fitting formulae have been provided to describe the $c - M$ relations from simulations ([Bullock et al. 2001](#); [Macciò et al. 2008](#); [Dutton & Macciò 2014](#); [Diemer & Kravtsov 2015](#)). Here we use the $c - M$ relation from [Prada et al. \(2012\)](#) to set the concentration for the satellite galaxies using their virial mass $M_{vir}(z_{acc})$ at accretion time z_{acc} . For the WDM model, it is found that the halo profile can still be described by the NFW profile (e.g., [Eke et al. 2001](#); [Schneider et al. 2012](#); [Macciò et al. 2013](#); [Lovell et al. 2014](#); [Schneider 2015](#); [Ludlow et al. 2016](#)), but the concentration, c_{WDM} , is generally reduced, and the $c_{WDM} - M$ relation is also non-monotonic, reaching a peak at a mass scale indicated by the truncation scale and decreasing at higher and lower masses. Here we use the fitting formula from [Schneider et al. \(2012\)](#) to describe the connection between the concentration c_{CDM} in CDM and c_{WDM} in WDM models,

$$\frac{c_{WDM}(M)}{c_{CDM}(M)} = (1 + 15 \frac{M_{hm}}{M})^{-0.3} \quad (5)$$

where M_{hm} is the half-mode mass which is related to the half radius, λ_{hm} , as $M_{hm} = \frac{4\pi}{3} \bar{\rho} (\lambda_{hm}/2)^3$, and λ_{hm} is the length scale at which the amplitude of the WDM transfer function (Eq. 1) is reduced to 1/2. A similar fitting formula for the $c - M$ relation in WDM is also provided in [Bose et al. \(2016\)](#).

As an illustration, in left panel of Fig. 2 we show the $c - M$ relation at $z=1$ for the CDM and WDM models. The colorful lines are predictions for WDM models. It is found that the fitting formulae from [Schneider et al. \(2012\)](#) and [Bose et al. \(2016\)](#) are very similar and their difference is less than 20% at $M_{vir} > 10^9 M_\odot$. For the following analysis we use the $c - M$ relation from [Schneider et al. \(2012\)](#). Compared with the $c - M$ relation in the CDM model, this relation at the low mass end in WDM is steeper and halo

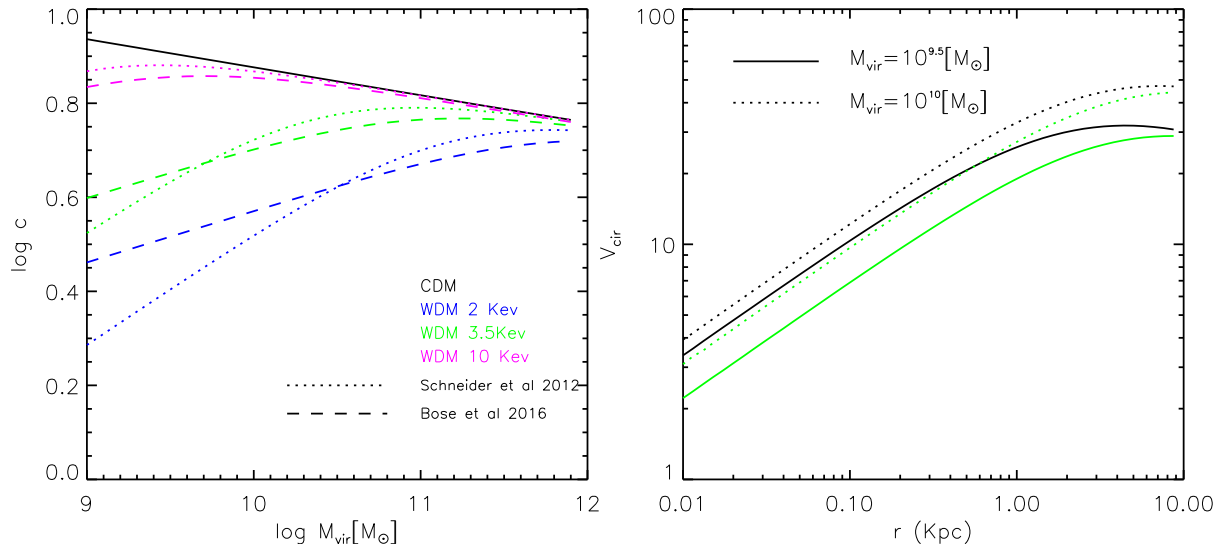


Figure 2. Left panel: the halo concentration-mass relations at $z=1$ for the CDM and WDM models. The black line is the fitting formula from Prada et al. (2012) for CDM. The color lines are for WDM models with $c - M$ relation from Schneider et al. (2012) and Bose et al. (2016), respectively. Right panel: the circular velocity of two NFW haloes at $z=1$ in the CDM (black lines) and WDM with mass $m_{\nu} = 3.5$ keV.

concentration is significantly decreased, depending on the WDM mass. At halo mass around $10^{10} M_{\odot}$, the concentration in WDM with $m_{\nu} = 3.5$ keV is around 63% of that in the CDM model. This decrease in c will result in a lower circular velocity, as shown in the right panel where we plot the circular velocity of two haloes at $z=1$ in both CDM and WDM model with $m_{\nu} = 3.5$ keV, respectively. This plot shows that in the CDM model halo circular velocity depends weakly on halo mass as the $c - M$ relation is relatively flat, but in the WDM model the halo mass dependence is stronger mainly due to the steeper $c - M$ relation at the low-mass end.

To model the baryonic feedback on the inner density slope of dark matter in satellite galaxy, we use the fitting formula by Di Cintio et al. (2014) which is only dependent on the star formation efficiency,

$$\alpha(x) = -0.06 - \log_{10}[(10^{x+2.56})^{-0.68} + (10^{x+2.56})] \quad (6)$$

where $x = \log_{10}(M_{*}/M_{\text{vir}})$, is the star formation efficiency given from the semi-analytical model or the halo AM method. Similar results have been obtained from other state-of-art hydro-dynamical simulations (e.g., Tollet et al. 2016; Fitts et al. 2017; Hopkins et al. 2018). To simply illustrate the dependence of α on the star formation efficiency in the galaxy, we plot this fitting formula in Fig. 3. It is seen that the baryonic effect peaks at around $M_{*}/M_{\text{vir}} \sim 0.005$ where the feedback energy is enough to redistribute the inner dark matter and create a flat profile. For low star formation efficiency with $M_{*}/M_{\text{vir}} < 10^{-4}$, the feedback energy is not enough to expel the dark matter distribution. For high star formation with $M_{*}/M_{\text{vir}} > 0.03$, the gravity from the excess stars in galaxy center will drag dark matter in and create a steeper profile.

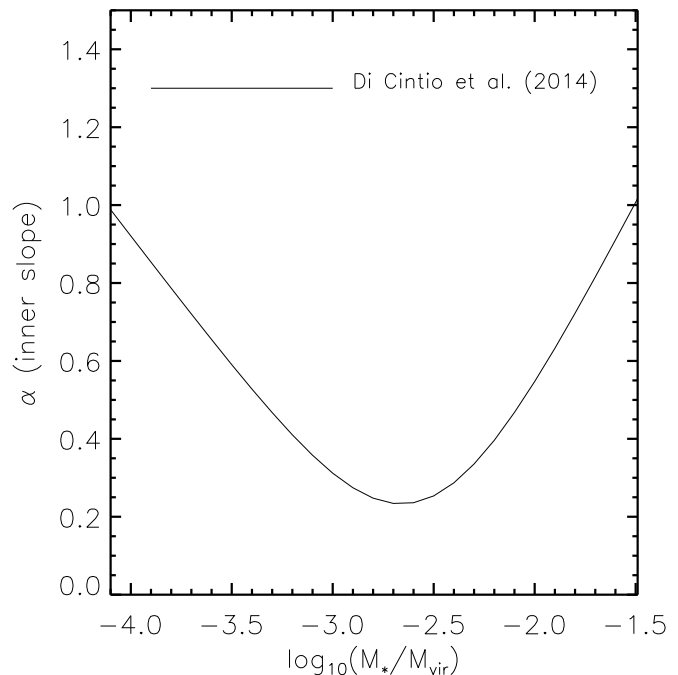


Figure 3. The impact of baryonic feedback on the inner dark matter density profile, α , as a function as the star formation efficiency, M_{*}/M_{vir} . The solid line is the fitting formula from Di Cintio et al. (2014)

2.4 Tidal effect on satellite mass and inner profile

The second process included in our model is the effect of tidal stripping on satellite inner structure. It has long been recognized that, after accretion, the strong tidal force from the host halo will strip the DM mass of the satellites and the associated tidal heating (or tidal stirring) will change their inner structure, leading to a decrease of dark matter mass and velocity dispersion (e.g., Gnedin et al. 1999). Ear-

lier studies (e.g., [Read et al. 2006](#)) claimed that the tidal effect is not strong enough to bring the satellites with initial cusp profile to match the data. It is later found that the tidal effect is more evident in satellites with initial flat slope and it can even lead to a total disruption of satellite galaxy (e.g., [Peñarrubia et al. 2010](#)). More recent simulations have shown that a combined effect from initial flat density profile and tidal heating can lower the circular velocity of satellites to agree with the data (e.g., [Brooks & Zolotov 2014](#); [Tomozeiu et al. 2016](#); [Frings et al. 2017](#)).

The tidal effect depends on the orbit of satellite and it is difficult to estimate the accurate degree of tidal reduction on satellites mass without exact information of its accretion time and infall orbit. Fortunately, in the simulation by [Peñarrubia et al. \(2010\)](#) they found that for satellite with given slope (α), the evolution of the structure parameters, such as r_{max} , V_{max} , can be better described solely by the amount of stripped dark matter mass. For halo with initial profile described by Eq. 4, [Peñarrubia et al. \(2010\)](#) provided a simple empirical formula to fit the evolution of the structure parameters as,

$$g(x) = \frac{2^\mu x^\eta}{(1+x)^\mu} \quad (7)$$

where $g(x)$ presents either $V_{max}/V_{max,0}$ or $r_{max}/r_{max,0}$, and $x = m_s/m_{s,0}$. Here $m_{s,0}$, $V_{max,0}$, $r_{max,0}$ are the halo mass, maximum circular velocity, corresponding radius of $V_{max,0}$ of satellites before accretion. [Peñarrubia et al. \(2010\)](#) listed a few fitted values of $\mu(\alpha)$ and $\eta(\alpha)$ for haloes with initial profile $\alpha = 0.0, 0.5$ and 1.0 . In the recent work by [Lovell et al. \(2017\)](#) and [Hiroshima et al. \(2018\)](#) to model subhalo evolution, they take the value of $\mu(1)$ and $\eta(1)$ by assuming the subhalo initially has NFW profile with $\alpha = 1$. In our model, the inner profile α of satellite before accretion is not fixed as $\alpha = 1$, but varies with the star formation efficiency, as given from Eq. 6. To apply Eq. 7 on any α , we use a linear interpolation to their best fitting values to get μ and η for any α determined from Eq. 6. Note that in the simulation of [Peñarrubia et al. \(2010\)](#) the inner slope α is assumed to be fixed during the subhalo evolution, but as V_{max} and r_{max} are changed, one has to rescale its ρ_0 and r_0 in Eq. 4 to solve the new r_{max} and V_{max} given by Eq. 7. The procedure is given in the Appendix A of the [Peñarrubia et al. \(2010\)](#) paper.

The above Eq. 7 depends on the mass loss of the satellite galaxy after accretion. Following [Kang \(2009\)](#), we use the orbit-average mass-loss rate given by [Giocoli et al. \(2008\)](#) to model the evolution of the subhalo mass,

$$\frac{dm}{dt} = -\frac{m}{\tau}(m/M_{host})^\zeta \quad (8)$$

where m and M_{host} are the dark matter mass of the satellite and the host. We tune the parameter τ and ζ to best fit the subhalo mass function from simulations (e.g., [Gao et al. 2004](#)). The free parameters (τ, ζ) in our model are (3 Gyr, 0.06), slightly different from those (2 Gyr, 0.07) in [Giocoli et al. \(2008\)](#). This is due to the different merger tree algorithm used in our study. Using the above equation it is found that on average subhaloes have lost 90% of their mass after accretion and the predicted mass-to-light ratio agrees well with the measured data ([Kang 2009](#)).

In Fig. 4 we show the examples of tidal stripping on the circular velocity profile of a NFW halo with mass $10^{10}M_\odot$

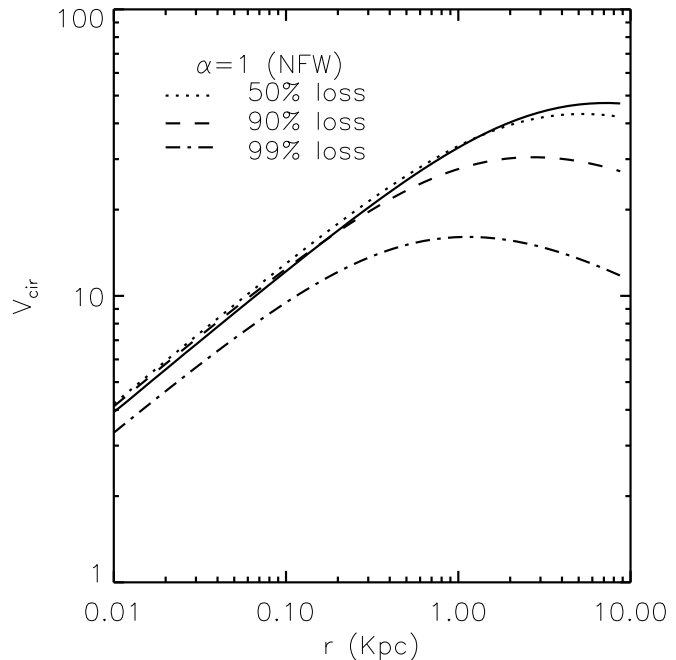


Figure 4. The effect of tidal heating on the circular velocity of subhalo. Here predictions are based on the [Peñarrubia et al. \(2010\)](#) simulations for a NFW halo with mass of $10^{10}M_\odot$ at redshift 1. Different lines are for different mass loss rate by tidal process.

accreted at redshift $z_{acc} = 1$. Different lines are for predictions with different fractions of mass loss. Note that here the fraction of mass loss is arbitrary set to show its effect on the circular velocity. It is seen that for subhalo with mass loss less than 90%, the circular velocity is almost not affected within $1Kpc$. In fact it is slightly higher in central region as the scale radius, r_s , is decreased with this fraction of mass loss. For subhalo losing 99% of its mass, the circular velocity is strongly reduced at all radii. We will later see that the very faint satellites, such as Canes Venatici and Ursa Minor, have lost more than 90% of their mass after accretion, so their circular velocity are strongly affected by the Milky Way tidal force. This is mainly due to the earlier accretion redshifts for faint satellites.

Now with the above formulae at hand, we are able to predict the circular velocities of the satellites after their accretion. We note that the above model has some limitations. The first is that we do not consider the scatter on the $c - M$ relation. The second is that the fitting formula, Eq. 6, for baryonic effect on the halo inner profile is obtained only from CDM simulation, while in WDM model, the halo concentration is lower and the change of inner profile due to baryonic feedback could be different. Nevertheless, [Macciò et al. \(2019\)](#) recently have shown that this effect is very weak in the WDM model, so we still use this fitting formula for the WDM case. Third, the exact tidal effect on subhalo inner structure is more complicated and should depend on the specific infall orbit, individual mass loss of each satellite galaxy, but here we use the average mass loss rate for subhalo accreted at given time and it should be viewed as an average effect.

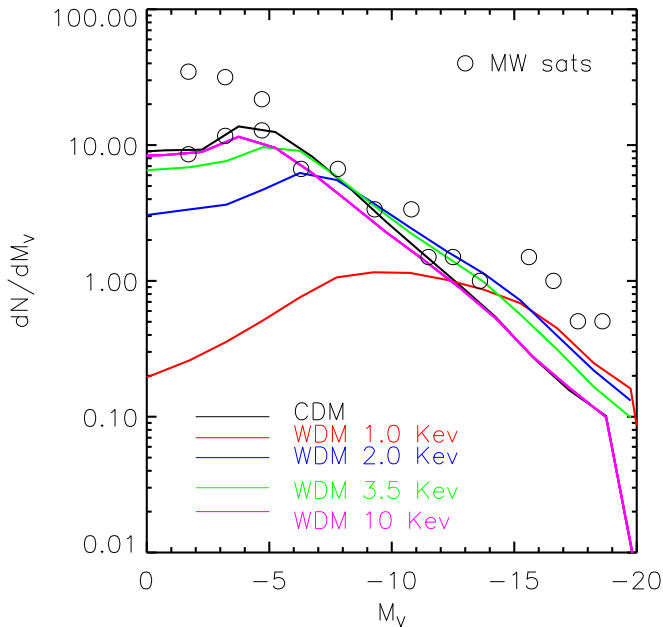


Figure 5. The luminosity functions of satellite galaxies in MW type halo from the CDM and WDM models. The empty circles are data from Kopeck et al. (2008) and lines are our model predictions. For each model, we have tried to tune the parameters for star formation and feedback to best match the data. The line styles are the same as those in Fig. 1. It is seen that $m_s = 1, 2$ keV models fail to match the MW data at the faint end.

3 RESULTS

3.1 satellite luminosity function

In the semi-analytical model, the free model parameters, such as star formation and supernova feedback efficiency, are often tuned to match the local observations, usually the stellar mass function and cold gas content (e.g., Kang et al. 2005; Guo et al. 2011; Luo et al. 2016). As the observational constraints on these free parameter are very weak, so they are coupled with the cosmological model and the dark matter properties. As shown in Kang et al. (2013), the observed stellar mass function at $M_* > 10^9 M_\odot$ can also be matched in the WDM model with $m_\nu > 1$ keV by tuning the model parameters, and the degeneracy can be broken by using other data, such as the Tully-Fisher relations. Here we tune the supernova feedback efficiency to best match the satellite luminosity function in both the CDM and WDM models. It is found that we can get a good match to the bright end of the luminosity function by setting the feedback efficiency as 0.02, 0.05, 0.1 and 0.3 for the WDM model with $m_\nu = 1, 2, 3.5$ and 10 keV. For the CDM model we set the feedback efficiency as 0.3.

In Fig. 5 we show the best matched satellite luminosity functions from the CDM and WDM models, respectively. In agreement with previous results (e.g., Kang 2009; Macciò et al. 2010), it is possible for the CDM to match the data up to $M_v = -5$. The data at $M_v > -5$ has larger uncertainty due to different assumptions on the intrinsic spatial distribution (NFW or isothermal) of satellite galaxies in the MW. In this work we will only focus on brighter satellites with $M_v < -5$. It is seen that for the WDM model with $m_\nu \sim 1 - 10$ keV, the bright end

of the luminosity functions can be roughly reproduced. In the semi-analytical model, galaxy stellar mass is very sensitive to the supernova feedback efficiency. As the formation of low-mass haloes in WDM model is suppressed, to form enough stars in low-mass haloes, we need to lower the feedback efficiency in those haloes. For example, in the WDM model with $m_\nu = 1$ keV, the supernova feedback efficiency is decreased to about 2%. Note that the feedback efficiency is highly uncertain, ranging between 0.1 to 0.5 adopted in different SAMs (e.g., Somerville & Primack 1999; Cole et al. 2000; Kang et al. 2005; Croton et al. 2006; Guo et al. 2011) and simulations (e.g., Li et al. 2017). From Fig. 5 it is seen that even with such a lower feedback, the WDM model with $m_\nu = 1$ keV still fails to reproduce the number of very faint satellites. The same behavior is also seen for the $m_\nu = 2$ keV model. The WDM model with $m_\nu \geq 3.5$ keV is able to reproduce enough faint satellite galaxies.

3.2 The host haloes of satellite galaxies

Using our model we are also able to predict the other properties of the MW satellites. For each observed satellite galaxy, we select its counterpart from each of the 5000 MW host galaxies. Here we define the model counterparts as those satellites having luminosity as the observed one. Note that the realistic counterparts of an observed satellite galaxy in the model should be those having the same luminosity and phase-space distribution (spatial position and motion) as the observed one. Since our model does not include the phase-space information, here we only use the luminosity to select model satellites. In Fig. 6 we show the distributions of the halo mass, star formation efficiency, and halo inner density slope at the infall time for model satellites corresponding to each of the nine classic satellites. The lower right panel shows the distributions of the accretion redshift. As in previous work, we have excluded the Large Magellanic Cloud and Small Magellanic Cloud from our analysis since the two massive satellites are rare in MW type haloes (e.g., Liu et al. 2011; Jiang et al. 2012). We also exclude Sagittarius galaxy as it is now in process of being disrupted. Here the model predictions are from CDM and satellites are ordered in decreasing luminosity with different colors, as labelled in the upper left panel.

It is clearly seen from upper left panel of Fig. 6 that in the SAM, more luminous satellites are on average living in more massive subhaloes. Most faint satellites, such as Leo II and fainter ones, stay in haloes with infall mass around $3 \times 10^9 M_\odot$. These predicted halo mass at infall agree well with those derived from hydro-simulation (Buck et al. 2019). The upper right and lower left panels show the star formation efficiency and associated inner DM density profiles. It is found that the star formation efficiency is also higher in the luminous satellites and the creation of shallow density profiles are stronger in these galaxies. It is interesting to see that the inner profile of satellite Leo I is strongly affected by the baryonic effect, as its star formation efficiency M_*/M_{halo} is around 0.002, close to the peak shown in Fig. 3.

In Fig. 7 we show the same predictions from the SAM in the WDM model with $m_\nu = 2$ keV and from the halo AM method in CDM model, in the upper and lower panels respectively. By comparing the semi-analytical predictions

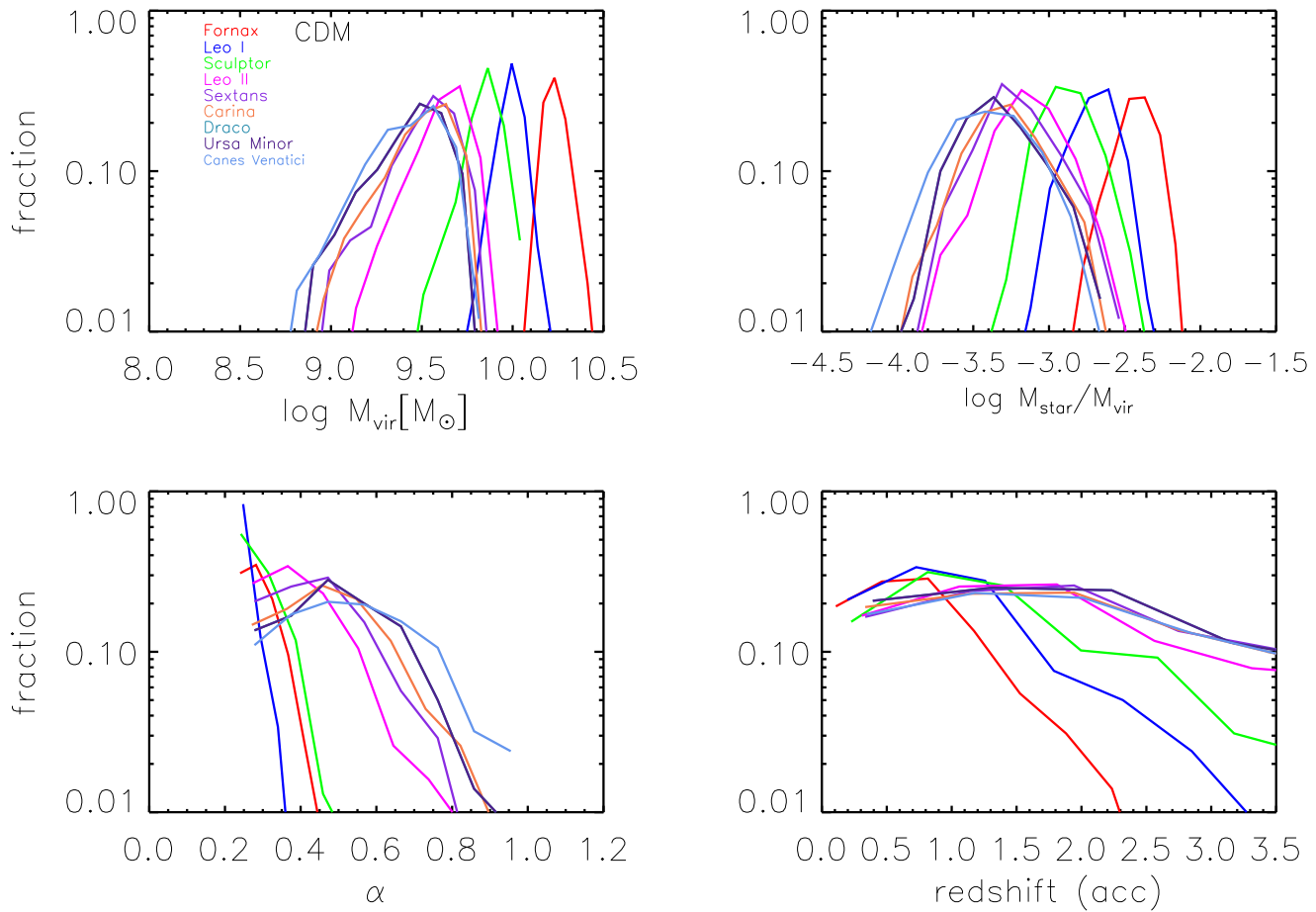


Figure 6. The predicted properties of bright satellite galaxies from the SAM. For each observed bright satellite, we select its counterparts, which have the same luminosity as the observed one, from our model satellite galaxies in the 5000 Milky Way host haloes. The upper left, upper right, lower left panels are for the distributions of the halo mass, star formation efficiency, inner density profile at infall time. The lower right panel shows the accretion redshifts. Each color line corresponds to one satellite galaxy as labelled in the upper left panel.

from the CDM and WDM models (Fig. 6 and upper panels in Fig. 7), it is found that the host halo mass of satellites from WDM is systematically lower by $0.2dex$ than that from the CDM model. This is not surprising, as in the WDM model the number of haloes is lower, so for given number density of subhalo, the average subhalo mass is lower by $0.1 \sim 0.3dex$ in the WDM 2.0 keV model, as can be seen from Fig. 1. Meanwhile, the host halo mass distribution is slightly wider in the WDM model. The decreases in host halo mass leads to a slightly higher and wider distribution of the star formation efficiency in the WDM model (second panel). For some fainter satellites, the star formation efficiency in WDM model is shifted to higher value than the peak, leading to a slightly steeper slope α .

By comparing the lower right panel of Fig. 6 with the upper right panel of Fig. 7, it is seen that in the WDM model, the accretion redshifts for satellite galaxies are slightly higher, especially for the brightest ones. This is mainly due to the lower host halo mass in the WDM and it is well known that in either WDM or CDM, low-mass haloes form earlier. Overall, the host halo mass and accretion time of satellites from the WDM 2.0 keV model and the CDM are not significantly different, and we will later see that it

is mainly the difference in the halo concentration leading to the low circular velocity in the WDM model.

The lower panels in Fig. 7 show the predictions from the halo AM in the CDM model. As noted before, we assign the measured stellar mass of the nine classic satellites (see Migheli & Hilker 2011 and references therein) to the most massive nine subhaloes in the model. Note that we have omitted the two most massive subhaloes in each host halo from our model, as they are thought to hold the LMC, SMC. It is seen that the distributions are significantly different from those in Fig. 6. Firstly, the host halo mass of satellites in the AM model are on average larger than those in the SAM, and the mass distribution becomes narrower. This is not surprising from the AM method. For most of the faint satellites, the star formation efficiency in the AM model is lower, mainly due to the higher host halo mass. Secondly, the inner density profile of satellite (α) is now on average more close to NFW, as the star formation efficiency and the associated feedback is now lower in the AM model. Thirdly, the accretion redshifts of satellites are lower, with most are accreted below redshift 3.5, while in the SAM some satellites are accreted at much earlier times. One consequence of the later accretion redshift means the effect of tidal stripping, both dependent on the subhalo mass and inner mass distribution, is weaker

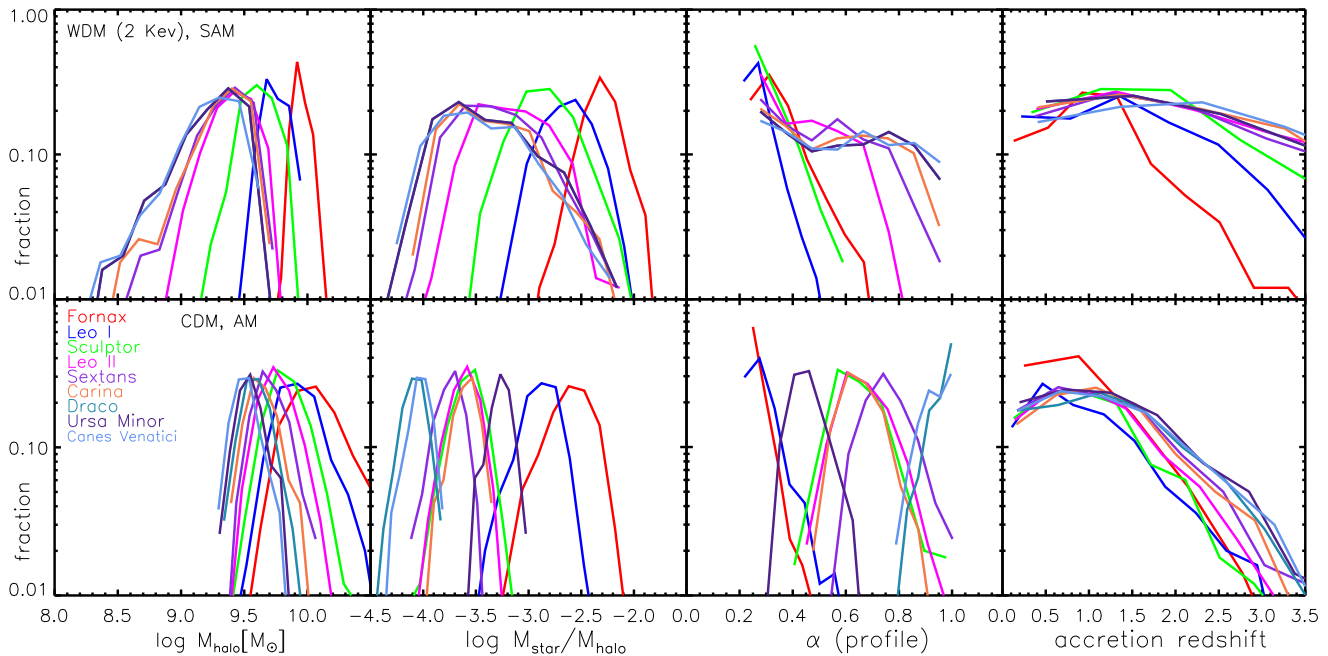


Figure 7. The same as in Fig. 6, but for the WDM model with $m_s = 2$ keV (upper panel). The lower panel is for CDM but where the satellites are selected using the abundance matching method so that the brightest satellites (with their observed stellar mass) are assigned to the most massive subhaloes at accretion.

in the AM model. Thus we will later see that the decrease of circular velocity of satellites by baryonic feedback or tidal heating in the AM model is weaker than that in the SAM.

We note that some of the above results, such as satellites infall time, are not comparable to those derived from the real data. One important caveat is that we do not have the phase-space information of the satellites, but only the stellar mass of the satellites. Rocha et al. (2012) have tried to derive the infall times for MW satellites based on their dynamical properties. They found that Carina, Ursa Minor and Sculptor were accreted more than 8 Gyr ago ($z > 1$). Fornax is recently accreted around ~ 2 Gyr ago. The remaining other satellites, including Sextans and Segue 1, are probably accreted early, but with larger uncertainty. Using Gaia data the infall times and orbits for most satellites have been recently updated (Fritz et al. 2018; Fillingham et al. 2019). Satellites in our SAM have on average higher accretion redshifts than the derived ones, but the general trend is qualitatively consistent with the data in the sense that faint satellites, such as Carina and Ursa Minor, have higher accretion redshifts than those luminous satellites. This is the consequence of two combined effects. First, faint satellites are more likely to form in low-mass haloes which were accreted more early in the CDM model. Second, in case of cosmic reionization, faint satellites forms more earlier as their host halo is capable of holding hot gas at earlier times.

3.3 satellite kinematics

In this section we compare the predicted kinematic properties of the satellites, namely the circular velocity, to the data. Observational work (e.g., Mateo 1998; Walker et al. 2009; Wolf et al. 2010; McConnachie 2012) have measured the half-light radii and velocity dispersions for most satel-

lite galaxies in the MW. Following the arguments of Boylan-Kolchin et al. (2011), we focus on the data for bright satellite galaxies with $L_V > 10^5 L_\odot$ which have more reliable measurements of stellar spectra and member identification. For each satellite we transfer the measured line-of-sight velocity dispersion to the circular velocity at the half radii ($r_{1/2}$), labeled as $V_o = \sqrt{3}\sigma_{los}$. The data of $r_{1/2}$ and σ_{los} for the nine bright satellites can be found from the paper by Wolf et al. (2010). We note that this mass estimate may suffer from a systematic bias, as is found in Campbell et al. (2017).

For each model satellite, we calculate the circular velocity at the half light radii, labelled as V_m , using the above prescriptions on the evolution of the density profile. As seen from previous section, the model counterparts of each observed satellites have a wide distribution of properties, such as infall mass, infall time and tidal stripped mass, so the predicted V_m will also have a range of values. To compare with the data, we get the median velocity, $V_{m,50}$, defined as the circular velocity at 50 percentage of the velocity distribution. We also obtained the spread of the velocity as,

$$\sigma_m = (V_{m,90} - V_{m,10})/2 \quad (9)$$

where $V_{m,90}$, $V_{m,10}$ is the circular velocity of model satellites at the 90 and 10 percentage of the distribution. To quantify the degree of agreement between the model prediction and the data, we adopt the reduced chi-squared (Andrae et al. 2010) as,

$$\chi_{red}^2 = \frac{1}{n} \sum \frac{(V_{m,50} - V_o)^2}{\sigma_o^2 + \sigma_m^2} \quad (10)$$

where σ_o is the uncertainty of the measured circular velocity of observed satellite, n is the total number of observed satellite galaxies. From the distribution of χ_{red}^2 and for 9 degree

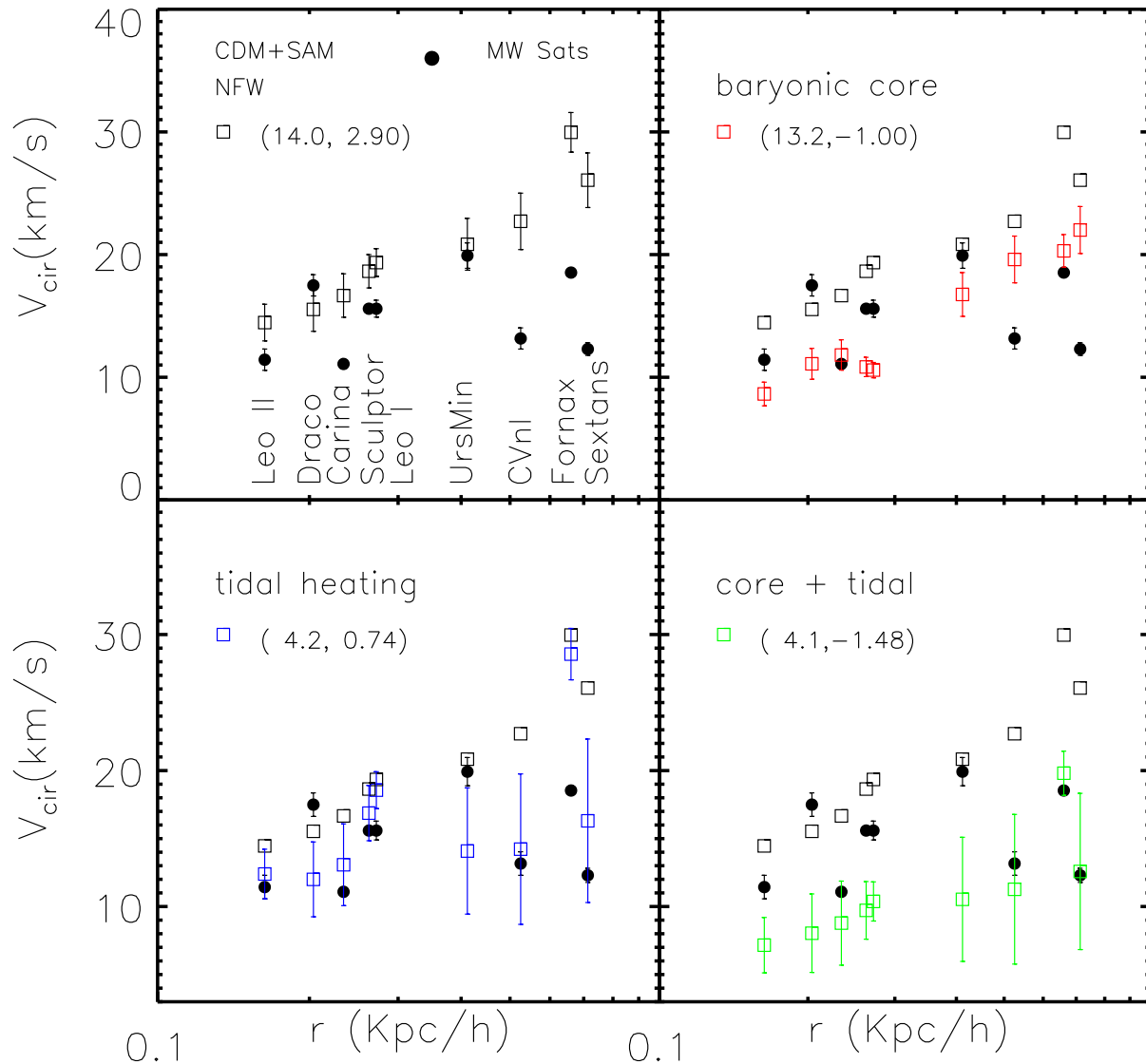


Figure 8. The circular velocity of satellite galaxies at the half-light radii. The black dots are the observational data. The squares in each panel are predictions from the semi-analytical model in the CDM model and the error bars are the velocity spread obtained from Eq. 9. For the black squares (replicated in all panels), satellite galaxies have NFW profile and no baryonic feedback or tidal heating effect included. The color squares in upper right and lower left show the results with only baryonic feedback or tidal heating effect included, respectively. The green squares in lower right have included both effects. In each plot, the degree of agreement between data and model, (χ_{red}^2, δ) , is also labelled.

of freedom (assuming the data of nine satellites are independent), the chance of a model matching the data with probability of 5%, 1% and 0.1% corresponds to $\chi_{red}^2 = 1.87, 2.4$ and 3.2. In this paper we select $\chi_{red}^2 = 3.2$ as an upper limit to exclude or accept a model. We note that given the systematics in our study, the choice of statistical significance should be taken as suggestive only. However, as χ_{red}^2 does not fully specify the agreement between the data and the model, here we define a mean deviation δ as,

$$\delta = \frac{1}{n} \sum \frac{(V_{m,50} - V_o)}{(\sigma_o^2 + \sigma_m^2)^{0.5}} \quad (11)$$

The defined δ quantifies the systematic deviation between the model and the data, in which $\delta > 0$ indicates the predicted circular velocity is systematically higher than the data. To place a rough limit on the agreement between model

and data, we set $\chi_{red}^2 = 3.2$ and $-1 < \delta < 1$ as the threshold to exclude a model. In each following plot we label the values (χ_{red}^2, δ) as a reference of how the model agrees with the data.

Now we compare the model predictions with the data. We show the circular velocity of the nine classic satellites at their half-light radii in Fig. 8, where we separate the effect of baryonic feedback and tidal heating in different panels. The black circles are the data for observed satellites (e.g., [Wolf et al. 2010](#)). The squares in each panel are the model predictions from our SAM in the CDM model with error bars showing the velocity spread obtained from Eq. 9. The black squares in the upper left panel are for satellites with NFW density profiles, with neither baryonic feedback nor tidal heating included, and they are replicated in other

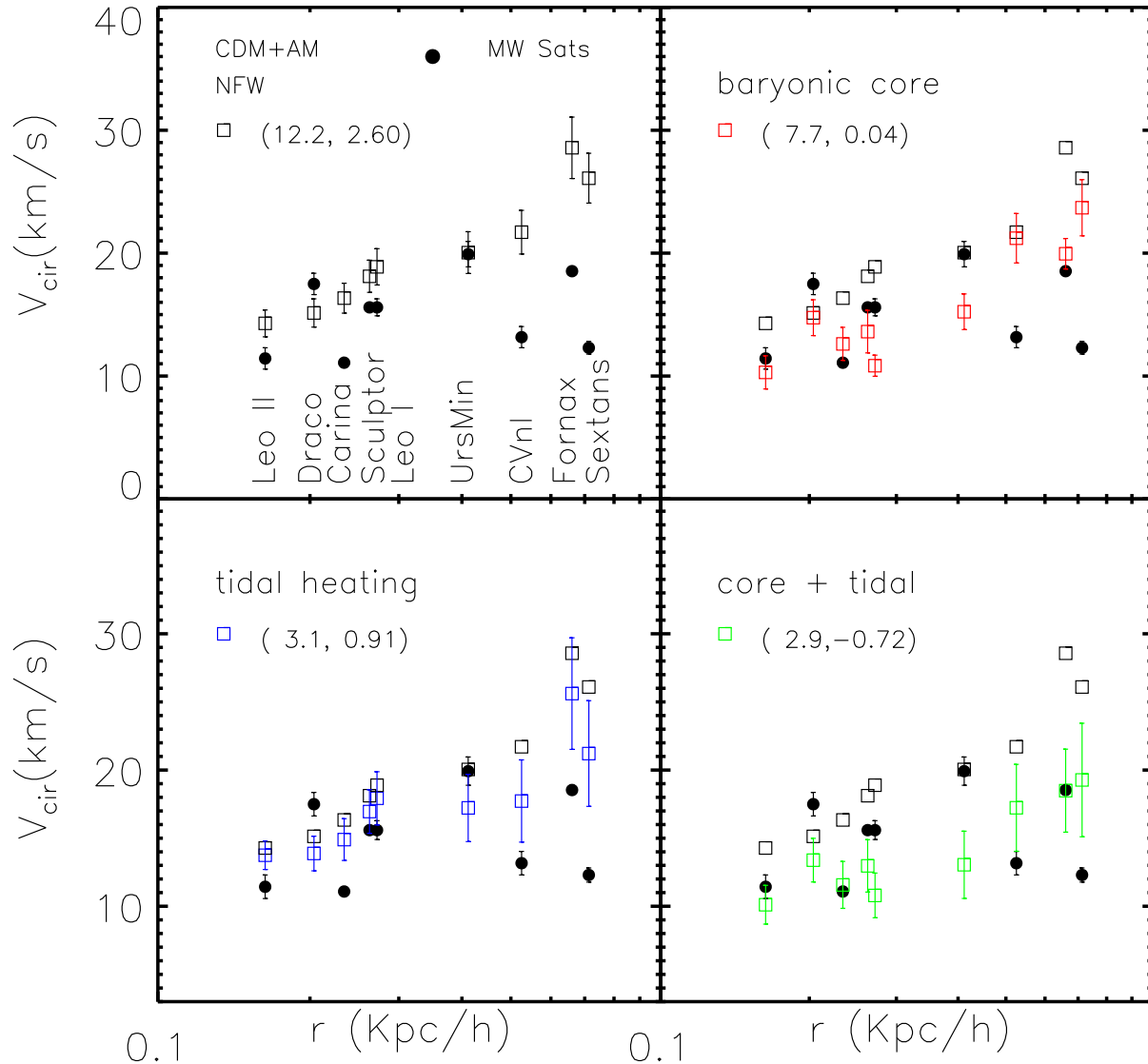


Figure 9. As in Fig. 8 for the CDM mode, but here the satellite galaxies are selected based on their halo mass at accretion. Compared to the predictions from the SAM in Fig. 8, it is seen that the baryonic feedback and tidal heating effects are both weaker. This is because satellites are now living in more massive subhaloes, thus both the star formation efficiency and accretion redshifts are also lower.

panels (no errorbar). In the upper right panel only baryonic feedback, or equally the new profile given from Eq. 6, is included. In the lower left panel, only the effect of tidal stripping and heating from Eq. 7 is included. Note that here no baryonic feedback is included, so each subhalo has a NFW profile ($\alpha = 1$). In the lower right panel, both effects are included. In this case, we firstly consider the effect of baryonic feedback, obtaining a star-formation dependent α , and then include the tidal heating. This is reasonable as star formation in satellites is often strongly suppressed after infall. As shown in Peñarrubia et al. (2010), the tidal effect on satellites inner structure depends on the initial profile α , with more strong effect for lower α , thus the predictions in the lower right panel is not the sum of the two effects in the upper right and lower left panel, but being slightly stronger.

Fig. 8 shows that in the CDM model the predicted circular velocities of model satellites with neither baryonic feedback nor tidal heating are systematically higher than ob-

served (upper left panel). In particular, the disagreement is more severe for the satellite Carina, CVnI, Fornax and Sextans. This was already clearly shown by many previous studies (e.g., Boylan-Kolchin et al. 2011; Wetzel et al. 2016). In fact these four satellite galaxies are the main drivers of the TBTF problem, as they contribute mostly to the relative flat distribution of the circular velocities. With only baryonic feedback included (red squares in the upper right panel), it is seen that the feedback does reduce the circular velocities by creating shallow profiles in some satellite galaxies. The degree of decrease varies among the satellites. For example, it is prominent in Leo I, but weak in UrsMin and CVnI. This is due to the relation between density profile α and the star formation efficiency in the satellites, as can be seen from Fig. 6. For some satellites, such as Carina and Fornax, the baryonic feedback leads to better agreement between the model and the data. However, for other satellites, the baryonic feedback is too strong, leading to the circular velocity

being lower than the data. The values of the statistical measures we set to compare with the data ($\chi_{red}^2 = 13.2$, $\delta = -1$) shows that the agreement between data and model is still not very satisfying.

By only including the tidal heating (blue squares in lower left panel), it is seen that the velocity distribution is now much flatter, in better agreement with the data, as also indicated by the statistical measures ($\chi_{red}^2 = 4.2$, $\delta = 0.74$). In particular the circular velocities of Carina, CVnI and Sextans are strongly decreased to match the data. This seems to suggest that tidal heating is the main factor to solve the high circular velocity of the main drivers of the TBTF problem. In this case, we should expect to see clear tidal feature in these satellite galaxies. However, observational determination of tidal feature in satellites is difficult and studies (e.g., Lokas et al. 2012) have shown that some satellites, such as Carina, have experienced strong tidal stirring. Roderick et al. (2016) found that tidal disruption is not prominent for Sextans, but tidal stirring effect could still be present. We will briefly discuss this in the final section. Note that the error bar in presence of tidal heating is larger than those from the baryonic feedback. This is because the distribution of satellite accretion time is wider, leading to a wider range of mass stripping and associated tidal heating. More interesting results are seen in the lower right panel where both baryonic feedback and tidal heating are included. Now the predicted satellite velocity is systematically lower than the data, as indicated by the value $\delta = -1.48$. Apparently, the problem is now reversed, from TBTF to too-diffuse-to-pass, as mentioned in previous studies (Dutton et al. 2016). This is mainly due to the strong feedback effect in this model, and we will discuss more in the last Section.

Now we investigate the results from the AM method in the CDM model, shown in Fig. 9. As previously shown, the main change in the AM method is that on average the host subhalo mass is larger than those in the SAM. The higher subhalo mass leads to two main consequences. First, the accretion redshifts of subhaloes are lower, thus the tidal stripping effect, depending on time after infall, is weaker in this model. Second, the star formation efficiency is now lower, thus the halo inner density profile α is more close to NFW. The upper left panel shows that in this model, the circular velocity distribution is very similar to that in the SAM. This is not surprising, as we have shown in Fig. 2 that in the CDM model the $c - M$ relation in the CDM model is relatively flat.

The upper right panel in Fig. 9 shows that with baryonic feedback, some satellites will have lower velocities than the data, such as the Sculptor and Leo I. Overall, the baryonic effect in this AM method is weaker than that in the SAM, and the fitted value ($\chi_{red}^2 = 7.7$, $\delta = 0.04$) indicates that the model is still inconsistent with the data. With careful inspection, we find that for the satellites mainly responsible for the TBTF problem in the MW, such as CVnI and Sextans, the baryonic effect is negligible and the model predictions for them are still away from the data. However, with tidal heating effect included, as shown in the lower left panel, it is seen that the model predictions agree slightly better with the data, either for each single satellite or the overall distribution. With both baryonic feedback and tidal heating

included, the velocity distribution shown in the lower right panel is more flat, more consistent with the data.

Overall, our above results show that in the CDM model, the effects of baryonic feedback and tidal heating depend on the model for galaxy formation. In the SAM, the host subhaloes of satellites have wide distributions in mass and accretion redshifts, giving rise to stronger baryonic feedback and tidal heating effects. In this case, the predicted circular velocity of satellite galaxies are systematically lower than the data. In the AM model, satellites form in most massive subhaloes, so the effects of baryonic feedback and tidal heating are modest. However, in both cases, it is found that tidal heating effect must be invoked to lower the circular velocities of some satellites, such as CVnI and Sextans, which are thought to be the main drivers of the TBTF problem.

3.4 Satellites kinematics with warm dark matter

As mentioned in the introduction, WDM model is proposed as an alternative solution to the TBTF problem. However, most existed studies using WDM model often neglected the effect of baryonic feedback and tidal effect, but see recent studies by Bozek et al. (2019) and Macciò et al. (2019). The analysis made in the previous section has shown that the baryonic feedback and tidal effects depend on how we selected satellites. In the AM method those effects are minimized as satellites are from the massive subhaloes which on average have lower accretion redshifts and weak baryonic feedback effect (due to their high halo mass). Thus, the AM case is a reasonable benchmark that could provide a conservative (in terms of the impact of baryonic feedback) lower limit in the WDM mass. Thus in this section, we use the AM method and apply it to the WDM model to set a lower limit on the WDM mass. Here we only consider three cases with $m_\nu = 2, 3.5, 10$ keV. We do not show the results for $m_\nu = 1$ keV as it can be ruled out just from the satellite luminosity function shown in previous section. Also note that in this part we fix the host halo mass as $10^{12} M_\odot$ and we will discuss the implications of other host halo mass in section 3.5.

We firstly show the results from the WDM model with $m_\nu = 2$ keV in Fig. 10. Similar to Fig. 9, we isolate the baryonic feedback and tidal heating in different panels. In the upper left panel where the dark matter density profile is modelled as NFW, we also add additional predictions using the black triangles, in which we use the $c - M$ relation from the CDM model. This is purely for comparison between the CDM and WDM to see the effects of changing halo concentration. It is found that the triangles are very similar to the squares in Fig. 9, indicating that although the halo formation history is different in the WDM model, the circular velocity from NFW profile is very similar. This is mainly due to the flat $c - M$ relation in the CDM model. The squares show that the circular velocities of satellites can be greatly reduced due to lower concentration in the WDM case. However, the statistical measures ($\chi_{red}^2 = 13.8$, $\delta = -2.52$) in our results shows that the model predictions are still systematically lower than the data.

The upper left and lower right panels show the effects of baryonic feedback and tidal heating, respectively. It is found that the baryonic feedback is more strong than the tidal heating, resulting in satellite circular velocities too below the data. The lower right panel includes both effects. Ap-

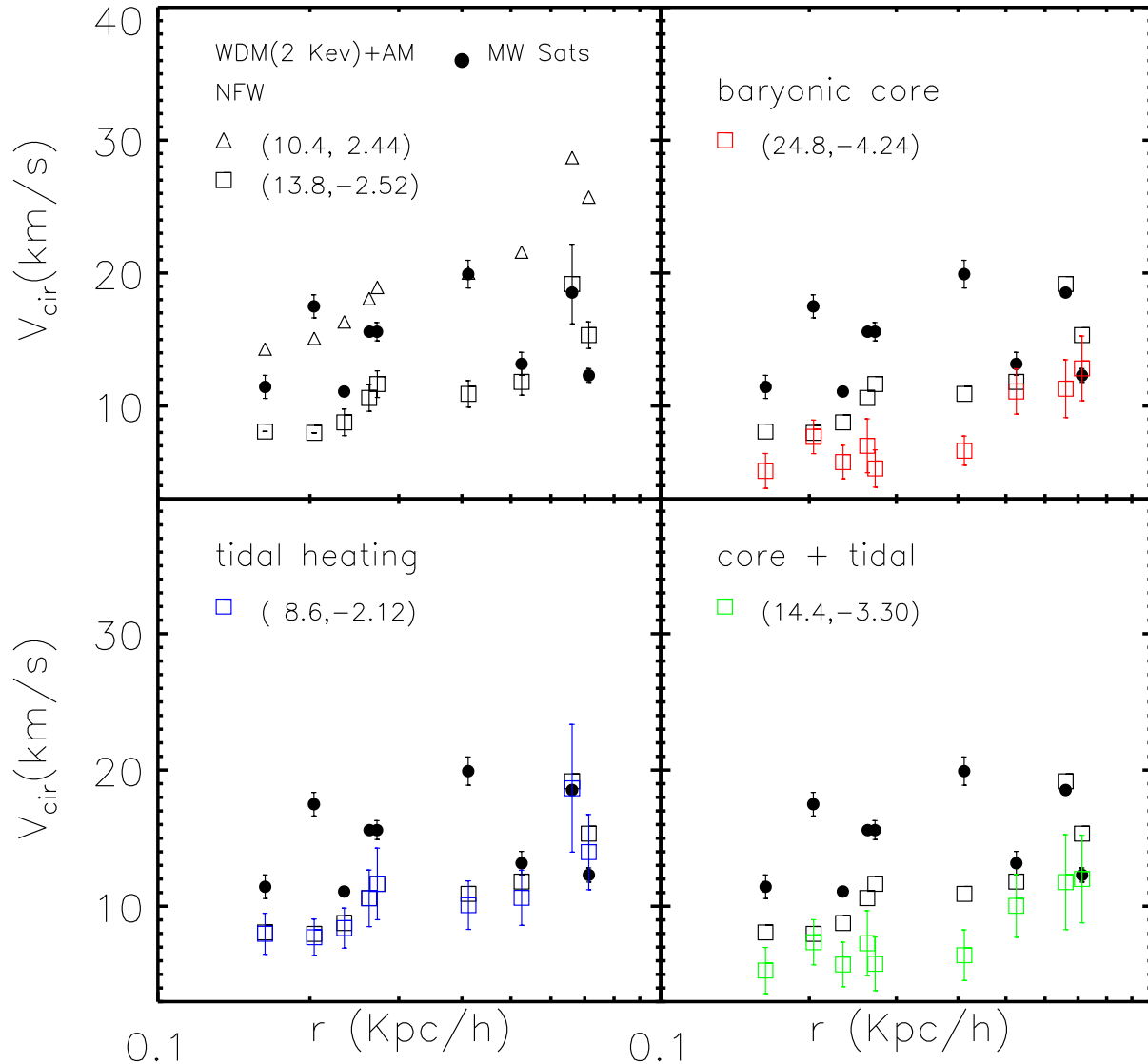


Figure 10. As in Fig. 9, but for the WDM model with $m_\nu = 2.0$ keV. Here in the upper left panel, we show additional predictions using the triangles in which the $c - M$ relation is the same as the CDM. So the comparison between triangles and squares directly shows the effect of halo concentration on circular velocity. The value of (χ_{red}^2, δ) in each panel indicates that the model predictions are systematically lower than the data.

parently, this plot shows that the WDM model with $m_\nu = 2$ keV can be safely ruled out. It indicates that in the 2 keV WDM model, any baryonic feedback effect and tidal heating is not tolerated, which is apparently implausible in reality.

We further show the results for two other WDM models with $m_\nu = 3.5, 10$ keV in Fig. 11. For the 3.5 keV model one can find the upper middle panel that with only tidal effect, the agreement between the model and the data is acceptable ($\chi_{red}^2 = 2.2, \delta = -0.48$). With both feedback and tidal included, the model predictions are systematically lower than the data, seen from the upper right panel. For WDM model with $m_\nu = 10$ keV, the model can match the data with inclusion of both baryonic feedback and tidal process, as seen from the lower right panel. This plot shows that for host halo mass of $M_{vir} = 10^{12} M_\odot$ the WDM model with $m_\nu \leq 3.5$ keV can be excluded if baryonic feedback and tidal heat-

ing are effective. Our model can not exclude the model with $m_\nu = 10$ keV.

3.5 The effects of host halo mass

For all results above we assume the MW has a halo mass of $10^{12} M_\odot$. Although most observational constraints on the MW mass are around this value, there is still uncertainty of a factor of 2 (Li et al. 2017; Callingham et al. 2019). For the WDM model with mass around a few keV, it is found from the satellite number count that the MW should have a mass larger than $10^{12} M_\odot$ (e.g., Kennedy et al. 2014). Here we test if the constraints from satellite kinematics in WDM model are consistent with previous conclusions.

In Fig. 12 we show the results for two MW mass, one is $1.5 \times 10^{12} M_\odot$ in the upper panels and one is $2 \times 10^{12} M_\odot$ in the lower panels. We do not test a MW halo mass lower

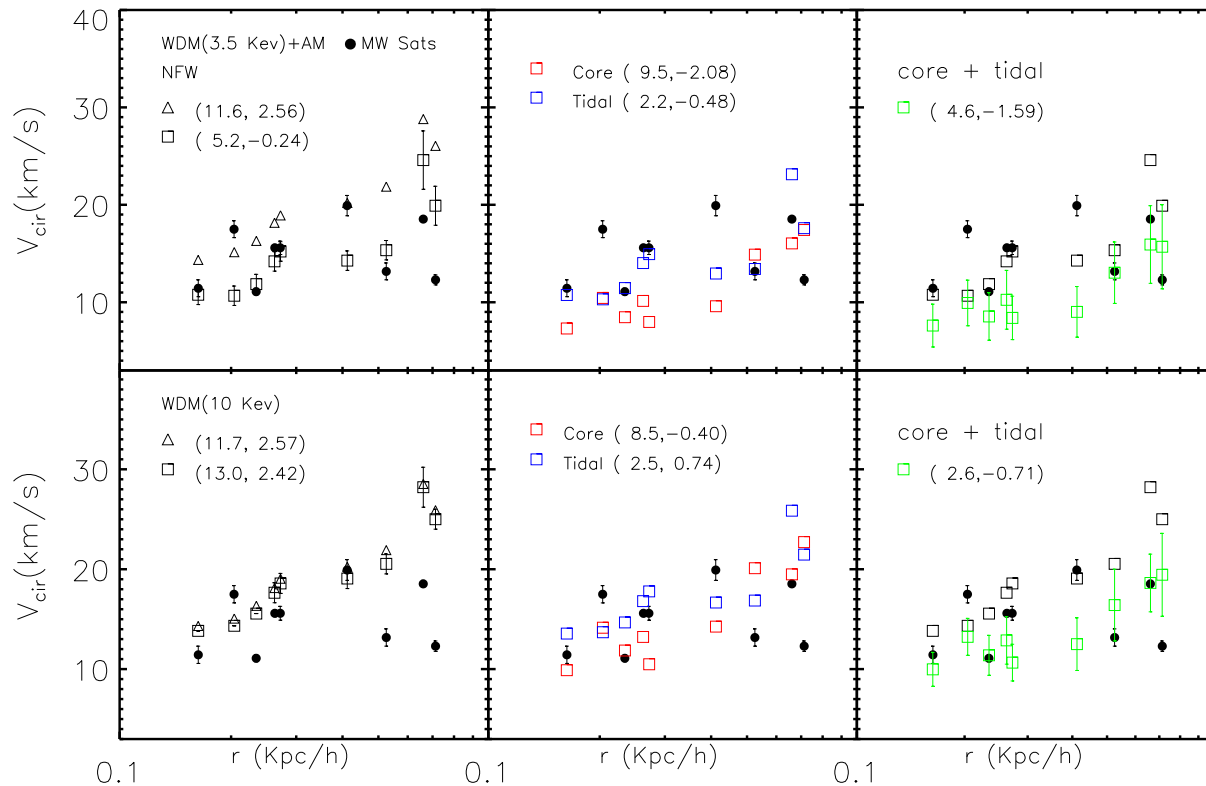


Figure 11. As in Fig. 10, but for two other WDM models with $m_\nu = 3.5, 10$ keV. It is seen that if both baryonic feedback and tidal heating are ineffective, the 3.5 keV WDM model is marginally acceptable. If both effects are in act, the 3.5 keV model can be excluded (for MW halo mass of $10^{12} M_\odot$), and the 10 keV model can not be excluded.

than $10^{12} M_\odot$ as it is seen from previous results that with a halo mass of $10^{12} M_\odot$, the CDM predictions is slightly lower than the data even in the AM method. The left, middle and right panels are for CDM, WDM with $m_\nu = 2.0, 3.5$ keV respectively. Here we do not show the 10 keV model as its predictions are close to the CDM results, and we only plot the model predictions with both baryonic feedback and tidal heating included.

We firstly investigate the effects of host halo mass in the CDM. By comparing the lower right panel of Fig. 9 with the left panels in Fig. 12, it is seen that MW with a slightly larger mass around $1.5 \times 10^{12} M_\odot$ agrees better with the data, with smaller χ^2_{red} and a δ close to 0. However, a more massive MW with mass of $2 \times 10^{12} M_\odot$ gives slighter higher circular velocity for satellites, beginning to depart from the data. It shows that, with inclusion of baryonic feedback and tidal heating, a MW with mass around $1.5 \times 10^{12} M_\odot$ agrees better with the MW satellite kinematics in the CDM model.

For the WDM models as shown in the middle and right panels, it is seen that for WDM with $m_\nu = 2$ keV, a larger MW halo with mass of $2 \times 10^{12} M_\odot$ still predicts circular velocities systematically lower than the data. Using satellite number count as a constrain, Kennedy et al. (2014) found that the lower limit of MW mass is $1.7 \times 10^{12} M_\odot$. Our results show that the mass limit can be pushed to a higher value. For WDM model with $m_\nu = 3.5$ keV, the right panels show that a MW with mass of $1.5 \times 10^{12} M_\odot$ is acceptable, while a higher mass of $2 \times 10^{12} M_\odot$ gives slightly better agreement with the data. We do not test higher values of the MW mass, as $2 \times 10^{12} M_\odot$ is almost the upper limit from most

observational constraints. Also the work of Kennedy et al. (2014) shows that a higher MW mass larger than $2 \times 10^{12} M_\odot$ will produce more bright satellites than observed.

4 CONCLUSION AND DISCUSSION

In this paper, we present an analytical model to study the luminosity and kinematic properties of the Milky Way satellite galaxies. We use a Monte-Carlo method to produce formation history for a large sample of Milky Way type haloes with mass around $10^{12} M_\odot$, and use analytical models to assign stellar mass to the subhaloes. Our model includes two key process to describe the evolution of the satellite density profile. One is the baryonic feedback which can induce a shallow density profile depending on the star formation efficiency, as suggested by recent state-of-the-art hydrodynamical simulations. The other is the tidal stripping process which will gradually strip the dark matter mass of the satellite galaxy and the associated tidal heating will redistribute the inner mass of the satellite. With these descriptions, one is able to predict the circular velocity of the satellites and compare the model with the data. By applying the analytical model to both CDM and WDM models with different mass, we have obtained the following main results,

- In the CDM model, galaxy formation model including cosmic re-ionization effect to suppress the baryonic content in low-mass haloes can fit the luminosity function of the satellite galaxies in the Milky Way. By tuning the model parameters for star formation and feedback, the WDM models

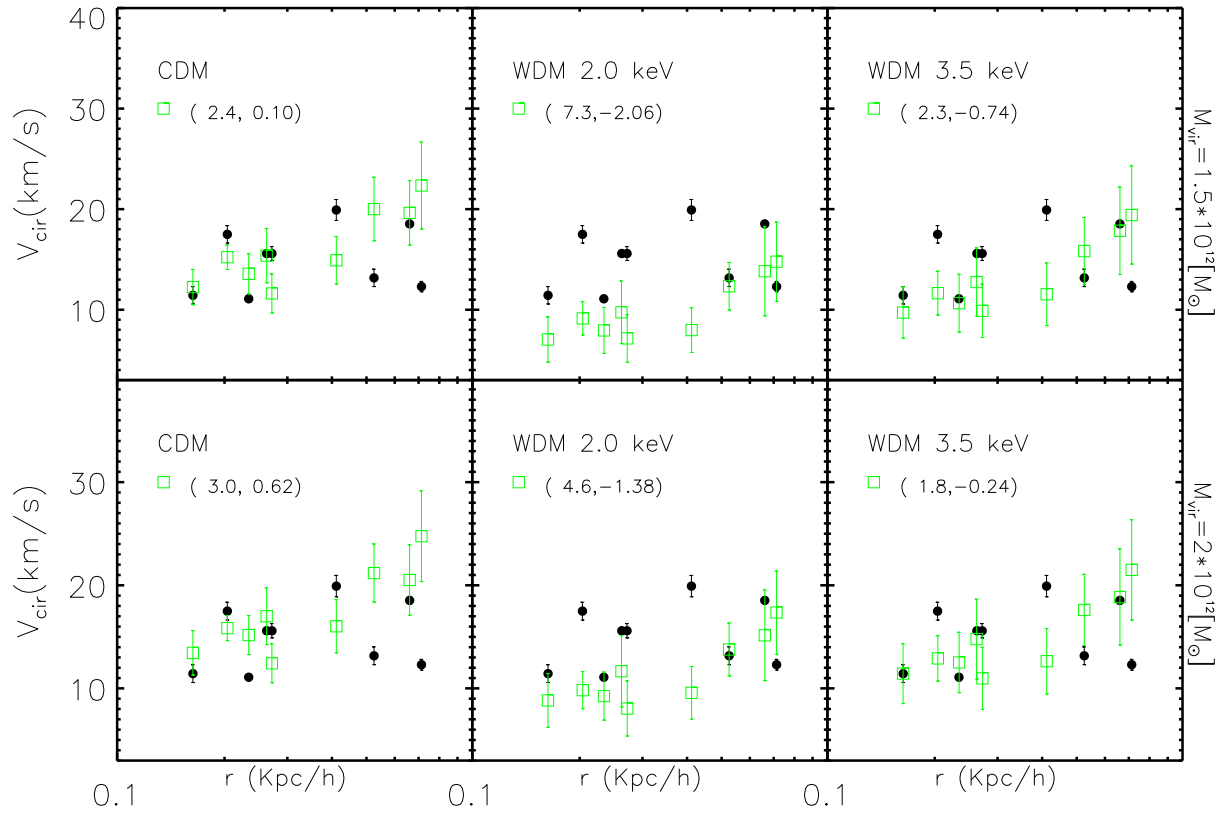


Figure 12. The effects of higher host halo mass on satellite circular velocities. Here both baryonic feedback and tidal heating are included. The upper and lower panels are for two MW halo mass with $1.5 \times 10^{12} M_{\odot}$ and $2 \times 10^{12} M_{\odot}$ respectively. For the CDM model, a lower MW halo mass is favoured. The WDM model with 2 keV mass can be excluded in both cases and for WDM with 3.5 keV, it requires the MW halo mass to be larger than $1.5 \times 10^{12} M_{\odot}$.

with $m_{\nu} > 2$ keV can reproduce the luminosity distribution of bright satellites ($M_V < -5$), but a lower mass with $m_{\nu} \leq 2$ keV fails to produce enough faint satellites and can be excluded.

- In the CDM model, by assuming that satellite galaxy initially follows NFW profile and neglecting the baryonic feedback and tidal process, the predicted circular velocities of the bright satellites are systematically higher than the data, in agreement with previous studies. The main drivers of this discrepancy between data and model (or the TBTF problem) are Carina, CVnI, Fornax and Sextans. By invoking only baryonic feedback in our model (semi-analytical or halo abundance matching), some satellites are predicted to have circular velocities, which are too low to be consistent with the data, while some satellites, such as CVnI and Sextans, always have high circular velocity than the data. It is found that tidal heating must be efficient to reduce the circular velocities of the main driver of TBTF, so as to agree with the data. The effect of tidal heating is in agreement with the findings from hydro-dynamical simulations (e.g., Garrison-Kimmel et al. 2019).

- In agreement with previous results (e.g., Kennedy et al. 2014) based on satellite number count, the constraint on WDM mass depends on the host halo mass. For MW with halo mass around $10^{12} M_{\odot}$, the WDM model with $m_{\nu} = 2$ keV can be excluded as the circular velocity of satellite galaxies are systematically lower than the data, even without any baryonic feedback or tidal heating. This is mainly

because the halo concentration in this WDM case is too low. For model with $m_{\nu} = 3.5$ keV, the model prediction marginally agrees with the data if baryonic feedback and tidal heating are both ineffective. If both effects are in play, the MW halo mass should be larger than $1.5 \times 10^{12} M_{\odot}$. Our current model can not exclude the 10 keV WDM model.

Here we briefly discuss the limitation and implication of our results. Our model has two important inputs to describe the evolution of the inner structure of satellite galaxy. One is that the inner density slope is modified from initial NFW ($\alpha = 1$) to a flat one by the baryonic feedback in the galaxy. The other is the tidal effect on the redistribution of the inner mass of satellite. Both descriptions have their limitation and uncertainties. For the first one, while some state-of-the-art hydrodynamical simulations, such as MaGICC, NIHAO and FIRE, have found that the density slope is correlated with the star formation efficiency, other studies like APOSTLE have not found the creation of a flat profile in satellite galaxy by baryonic feedback. The difference is contributed by a few factors, such as the subgrid physics implemented in these simulations, the star formation history or even the nature of dark matter. For more discussion on this issue, readers are referred to Bose et al. (2019).

Once baryonic feedback is inefficient to flatten the density profile in model satellites, one must consider how to lower their circular velocities, especially for the satellite Carina, CVnI and Sextans. One possibility is that these satellites are outliers and they could form in haloes with lower

concentration. One immediate consequence is whether the low-concentration subhaloes are able to survive the strong tidal force of the host halo. Another possibility is related to the second important ingredient of our model that tidal process can modify their inner mass distribution. For this purpose, we use the simulation results of [Peñarrubia et al. \(2010\)](#) to describe the effect of tidal heating. In their model it is found that the effect of tides on subhalo mass distribution is solely controlled by the total stripped mass fraction. The mass stripping depends on the orbit of the satellite galaxy. In our model we do not have the phase-space information of each subhalo but using an orbit-average mass loss rate for all subhaloes. In reality the mass stripping in the satellites could be different, leading to uncertainty on the predicted circular velocity.

Nevertheless, one robust conclusion of our model is that in the CDM, one must need tidal heating to lower the circular velocities of some satellite galaxies, such as Carina, CVnI and Sextans, to match the data. One will then expect to see the tidal feature in these satellites. As mentioned before, tidal stirring feature is clearly seen in Carina ([Lokas et al. 2012](#)), but is uncertain in Sextans ([Roderick et al. 2016](#)). As mentioned in these studies, unlike the satellite in the process of distinct disruption, such as Sagittarius, tidal features in normal low-surface dwarfs are very weak and has to be distinguished with their intrinsic bar structures. Current constraints are mainly from the optical data which are not deep enough. More observational data, including both optical and radio, are required to identify the tidal feature in the satellite galaxies, so as to quantify the extent of tidal heating on the inner structure of the satellite galaxies.

5 ACKNOWLEDGMENTS

We thank Shaun Cole for kind help on the Monte-Carlo merger tree code in the WDM case. We also thank the anonymous referee for constructive and thoughtful suggestions to improve the paper. The work is supported by the 973 program (No. 2015CB857003), the NSFC (No. 11825303, 11861131006, 11333008).

REFERENCES

- Andrae R., Schulze-Hartung T., Melchior P., arXiv:1012.3754
- Bardeen J. M., Bond J. R., Kaiser N., Szalay A. S., 1986, ApJ, 304, 15
- Benson A., Farahi A., Cole S., Moustakas J., Jenkins A., Lovell M., Kennedy R., Helly J., Frenk C. S., 2013, MNRAS, 428, 1774
- Bode P., Ostriker J., Turok N., 2001, ApJ, 556, 93
- Bose S., Hellwing W., Frenk C. S., Jenkins A., Lovell M., Helly J., Li B., 2016, MNRAS, 455, 318
- Bose S., et al., 2019, MNRAS, 486, 4790
- Boylan-Kolchin M., Bullock J.S., Kaplinghat M., 2011, MNRAS, 415, L40
- Bozek B., et al., 2019, MNRAS, 483, 4086
- Brooks A. M. & Zolotov A., 2014, ApJ, 786, 87
- Brook C., & Di Cintio A., 2015, MNRAS, 450, 3920
- Buck T., Macciò A. V., Dutton A., Obreja A., Frings J., 2019, MNRAS, 483, 1314
- Bullock J. S., Kolatt T.S., Sigad Y., Somerville R.S., Kravtsov A. V., Klypin A., Primack J. R., Dekel A., 2001, MNRAS, 321, 559
- Bullock J. S. & Boylan-Kolchin M., 2017, ARA&A, 55, 343
- Callingham T., et al., 2019, MNRAS, 484, 5453
- Campbell D., et al., 2017, MNRAS, 469, 2335
- Cole S., Lacey C. G., Baugh C. M., Frenk C. S., 2000, MNRAS, 319, 168
- Cole S., Helly J., Frenk C. S., Parkinson H., 2008, MNRAS, 383, 546
- Colin P., Avila-Reese V., Valenzuela O., 2000, ApJ, 542, 622
- Croton D. J., et al., 2006, MNRAS, 365, 11
- Cyr-Racine F.-Y., Sigurdson K., Zavala J., Bringmann T., Vogelsberger M., Pfrommer C., 2016, PhRvD., 93, 123527
- Di Cintio A., Brook C., Dutton A., Macciò A. V., Stinson G., Knebe A., 2014, MNRAS, 441, 2986
- Diemand J., Kuhlen M., Madau P., Zemp M, Moore B., Potter D., Stadel J., 2008, Nature, 454, 735
- Diemer B. & Kravtsov A. V., 2015, ApJ, 799, 108
- Dutton A. & Macciò A. V., 2014, MNRAS, 441, 3359
- Dutton A., Macciò A. V., Frings J., Wang L., Stinson G., Penzo C., Kang X., 2016, MNRAS, 457, 74
- Einasto J., 1965, Trudy Inst. Astroz. Alma-Ata, 51, 87
- Eke V., Navarro J. F., Steinmetz M., 2001, ApJ, 554, 114
- Errani R., Peñarrubia J., Walker M., 2018, MNRAS, 481, 5073
- Fillingham S., et al., arXiv:1906.04180
- Fitts A., et al., 2017, MNRAS, 471, 3547
- Frings J., Macciò A. V., Buck T., Penzo C., Dutton A., Blank M., Obreja A., 2017, MNRAS, 472, 3378
- Fritz T., Battaglia G., Pawlowski M., Kallivayalil N., van der Marel R., Sohn S., Brook C., Besla G., 2018, A&A, 619, 103
- Gao L., White S. D. M., Jenkins A., Stoehr F., Springel V., 2004, MNRAS, 355, 819
- Garrison-Kimmel S., et al., 2019, MNRAS, 487, 1380
- Garzilli A., Boyarsky A., Ruchayskiy O., 2017, PhLB, 773, 258
- Giocoli C., Tormen G., van den Bosch F. C., 2008, MNRAS, 386, 2135
- Gnedin O. Y., Hernquist L., Ostriker J. P., 1999, ApJ, 514, 109
- Gnedin N. Y., 2000, ApJ, 542, 535
- Governato F., et al., 2012, MNRAS, 422, 1231
- Grand R. J., et al., 2017, MNRAS, 467, 179
- Guo Q., et al., 2011, MNRAS, 413, 101
- Guo Q., Cooper A. P., Frenk C. S., Helly J., Hellwing W. A., 2015, MNRAS, 454, 550
- Hinshaw G., et al., 2013, ApJS, 208, 19
- Hiroshima N., Ando S., Ishiyama T., 2018, PhRvD, 97, 123002
- Hopkins P. F., ET AL., 2018, MNRAS, 480, 800
- Jiang C. Y., Jing Y. P., Li C., 2012, ApJ, 760, 16
- Jing Y. P. & Suto Y., 2000, ApJL, 529, 69
- Li M., Bryan G. L., Ostriker J. P., 2017, ApJ, 841, 101
- Liu L., Gerke B., Wechsler R. H., Behroozi P., Busha M., 2011, ApJ, 733, 62
- Lokas E. L., Majewski S. R., Kazantzidis S., Mayer L., Carlín J., Nidever D., Moustakas J., 2012, ApJ, 751, 61

- Kang X., Jing Y. P., Mo H. J., Börner G., 2005, *ApJ*, 631, 21
- Kang X., IAUS, 254, 32 (arXiv:0806.3279)
- Kang X., Li M., Lin W. P., Elahi P. J., 2012, *MNRAS*, 422, 804
- Kang X., Macciò A. V., Dutton A., 2013, *ApJ*, 767, 22
- Kennedy R., Frenk C. S., Cole S., Benson A., 2014, *MNRAS*, 442, 2487
- Klypin A., Kravtsov A., Valenzuela O., Prada F., 1999, *ApJ*, 522, 82
- Koposov S., et al., 2008, *ApJ*, 686, 279
- Kravtsov A. V., Gnedin O., Klupin A., 2004, *ApJ*, 609, 482
- Li Z-Z., Jing Y. P., Qian Y-Z., Yuan Z., Zhao D-H., 2017, *ApJ*, 850, 116
- Lovell M. et al., 2012, *MNRAS*, 420, 2318
- Lovell M., Frenk C. S., Eke V., Jenkins A., Gao L., Theuns T., 2014, *MNRAS*, 439, 300
- Lovell M., et al., 2017, *MNRAS*, 468, 4285
- Ludlow A., Bose S., Angulo R., Wang L., Hellwing A., Navarro J. F., Cole S., Frenk C. S., 2016, *MNRAS*, 460, 1214
- Luo Y., Kang X., Kauffmann G., Fu J., 2016, *MNRAS*, 458, 366
- Macciò A. V., Dutton A., van den Bosch F. C., 2008, *MNRAS*, 391, 1940
- Macciò A.V., Kang X., Fontanot F., Somerville R. S., Koposov S., Monaco P., 2010, *MNRAS*, 402, 1995
- Macciò A. V. & Fontanot F., 2010, *MNRAS*, 404, L16
- Macciò A. V., Ruchayskiy O., Boyarsky A., Muñoz, Cuartas J., 2013, *MNRAS*, 428, 882
- Macciò A. V., Frings J., Buck T., Dutton A., Blank M., Obreja A., Dixon K., 2019, *MNRAS*, 484, 5400
- Mateo M. L., 1998, *ARA&A*, 36, 435
- McConnachie A. W., 2012, *AJ*, 144, 4
- Misgeld I. & Hilker M., 2011, *MNRAS*, 414, 3699
- Moore B., Quinn T., Governato F., Stadel J., Lake G., 1999, *MNRAS*, 310, 1147
- Navarro J. F., Frenk C. S., White S. D. M., 1997, *ApJ*, 490, 493
- Ogiya G. & Burkert A., 2015, *MNRAS*, 446, 2363
- Parkinson H., Cole S., Helly J., 2008, *MNRAS*, 383, 557
- Peñarrubia J., Benson A. J., Walker M., Gilmore G., McConnachie A., Mayer L., 2010, *MNRAS*, 406, 1290
- Polisensky E. & Ricotti M., 2011, *PhRvD.*, 83, 043506
- Prada F., Klypin A. V., Cuesta A. J., Betancort-Rijo J., Primack J., 2012, *MNRAS*, 423, 3018
- Read J. I., Wilkinson M. I., Evans N., Gilmore G., Kleyna J., 2006, *MNRAS*, 367, 387
- Rocha M., Peter A., Bullock J., 2012, *MNRAS*, 425, 231
- Roderick T. A., Jerjen H., Da Costa G. S., Mackey A. D., 2016, *MNRAS*, 460, 30
- Sawala T., et al., 2016, *MNRAS*, 457, 1931
- Schneider A., Smith R., Macciò A. V., Moore B., 2012, *MNRAS*, 424, 684
- Schneider A., 2015, *MNRAS*, 451, 3117
- Shao S., Gao L., Theuns T., Frenk C. S., 2013, *MNRAS*, 430, 2346
- Simon J & Geha M., 2007, *ApJ*, 670, 313
- Simon J. D., 2018, *ApJ*, 863, 89
- Somerville R. S. & Primack J., 1999, *MNRAS*, 310, 1087
- Springel V., et al., 2008, *MNRAS*, 391, 1685
- Springel V., et al., 2005, *Nature*, 435, 629
- Stewart K., Bullock J., Wechsler R., Maller A., Zentner A., 2008, *ApJ*, 683, 597
- Tollet E., et al., 2016, *MNRAS*, 456, 3542
- Tomozeiu M., Mayer L., Quinn T., 2016, *ApJ*, 827, 15
- Vale A., Ostriker J. P., 2004, *MNRAS*, 353, 189
- Viel M., Becker G. Bolton J., Haehnet M., 2013, *PhRvD.*, 88, 043502
- Viel M., Lesgourgues J., Haehnelt M. G., Matarrese S., & Riotto A., 2005, *PhRvD*, 71, 063534
- Vogelsberger M., Zavala J., Loeb A., 2012, *MNRAS*, 423, 3740
- Vogelsberger M., Zavala J., Cyr-Racine F-Y., Pfrommer C., Bringmann T., Sigurdson K., 2016, *MNRAS*, 460, 1399
- Vogelsberger M., Zavala J., Schutz K., Slatyer T., 2019, *MNRAS*, 484, 5437
- Walker M. G., Mateo M., Olszewski E. W., 2009, *AJ*, 137, 3100
- Wang L., Dutton A., Stinson G., Macciò A. V., Penzo C., Kang X., Keller B., Wadsley J., 2015, *MNRAS*, 454, 83
- Wang W., Han J., Cooper A., Cole S., Frenk C. S., Lowing B., 2015, *MNRAS*, 453, 377
- Wetzel A. R., Hopkins P., Kim J., Faucher-Giguere C., Keres D., Quataert E., 2016, *ApJL*, 827, 23
- Wolf J., Martinez G. D., Bullock J., Kaplinghat M., Geha M., Muñoz R., Simon J. D., Avedo F., 2010, *MNRAS*, 406, 1220
- Zhao D. H., Mo H. J., Jing Y. P., Börner G., 2003, *MNRAS*, 339, 12
- Zolotov A., et al., 2012, *ApJ*, 761, 71

This paper has been typeset from a \LaTeX file prepared by the author.